ChemComm

AI-Designed RF Pulses Enable Fast Pulsing Heteronuclear Multiple Quantum Coherence NMR Experiment at High and Ultra-High Magnetic Fields

Journal:	*ChemComm*
Manuscript ID	CC-COM-10-2023-005370.R1
Article Type:	Communication

COMMUNICATION

AI-Designed RF Pulses Enable Fast Pulsing Heteronuclear Multiple Quantum Coherence NMR Experiment at High and Ultra-High Magnetic Fields

Received 00th January 20xx,
Accepted 00th January 20xx

DOI: 10.1039/x0xx00000x

Manu Veliparambil Subrahmanian and Gianluigi Veglia*

We present a new AI-optimized 2D Heteronuclear Multiple Quantum Coherence (RAPID-HMQC) pulse sequence for NMR spectroscopy. RAPID-HMQC is a longitudinal ^{1}H relaxation-optimized experiment with new AI-designed band-selective pulses to accelerate the analysis of organic compounds, metabolites, biopolymers, and real-time monitoring of dynamic processes at high- and ultra-high magnetic fields.

Two-dimensional heteronuclear NMR correlation experiments are widely used in structural and analytical chemistry to fingerprint small molecules, metabolites, and biopolymers. However, the sensitivity of this technique is severely affected by the low gyromagnetic ratios of heteronuclei (typically ^{15}N or ^{13}C). Longitudinal ^{1}H relaxation enhanced (LRE) experiments[1] have made it possible to acquire 2D experiments in a few seconds, enabling high-throughput screening and site-resolved, real-time characterization of kinetic processes. For instance, the Band-selective Excitation Short-Transient (BEST) family of experiments has accelerated the structural characterization of biopolymers such as proteins and nucleic acids at moderately high magnetic fields.[2-4] Among those experiments, band-Selective Optimized Flip-Angle Short-Transient heteronuclear multiple quantum coherence or SOFAST-HMQC has become the method of choice for the analysis of biomolecules and metabolites in living cell.[2, 3, 5-7] In the LRE experiments, hard (*i.e.*, rectangular) pulses are replaced by band-selective RF pulses[8] to irradiate only the desired spectral region (*e.g.*, amide resonances), avoiding the irradiation of water and aliphatic protons.[9] Under these conditions, the longitudinal relaxation rates obtained using band-selective pulses are shorter than those obtained using broadband pulses.[1, 9-11] Using this expedient, LRE experiments can operate with interscan delays ranging from 0.1 to 0.5 s, speeding up data acquisition. Yet, the most common band-selective pulses implemented in the SOFAST-HMQC experiment have limited irradiation bandwidth and inadequate compensation levels for pulse imperfections and RF inhomogeneity.[9] Although band-selective pulses can operate at larger bandwidths with increased RF power, this may result in a partial excitation of the water signal, whose intensity may exceed the receiver's dynamic range and reduce the overall sensitivity.[1, 9] Additionally, band-selective pulses exhibit non-uniform irradiation profiles, which can result in slightly different tip angles for ^{1}H resonances across the chemical shift range. These issues are exacerbated at high- and ultra-high magnetic fields, where the chemical shift breadth of all active nuclei is significantly broader. To resolve these issues, we used GENETICS-AI, GENErator of TrIply Compensated RF pulSes via Artificial Intelligence,[12, 13] to design novel band-selective pulses into the SOFAST-HMQC experiment. GENETICS-AI utilizes an evolutionary algorithm that continuously populates a library RF pulse shapes with different phase and amplitude profiles. To date, our library contains more than 1,000,000 RF pulses. The final RF shape is designed via an AI module from MATLAB® that is trained with the pulse shape library and generates optimal solutions based on specified parameters. A typical input for GENETICS-AI includes a) the target bandwidth, b) RF amplitude, c) level of inhomogeneity compensation, and d) operational fidelity.[12] The canonical scheme of the HMQC[14] experiment requires a pulse sequence 90°-Δ-180°-Δ-acquisition on the ^{1}H channel and a 90°-t_1-90°-decoupling[15] on the heteronucleus (^{15}N or ^{13}C). In the SOFAST-HMQC experiment,[3] the ^{1}H 90° and 180° pulses are replaced by two band-selective shapes, PC9[16] and REBURP, respectively.[17] The PC9 pulse[16] is calibrated to tip the magnetization at Ernst's angle,[18] which minimizes the interscan delay and increases the signal-to-noise ratio per unit time.[7] To achieve Ernst's angle, we programmed GENETICS-AI to generate a universal excitation pulse with a flip angle of 120°, UA120ev1, where the nomenclature indicates that this shapes operates a

Department of Biochemistry, Molecular Biology & Biophysics, and Department of Chemistry, University of Minnesota, Minneapolis, MN, 55455, USA. E-mail: vegli001@umn.edu

†Electronic Supplementary Information (ESI) available: [details of any supplementary information available should be included here]. See DOI: 10.1039/x0xx00000x

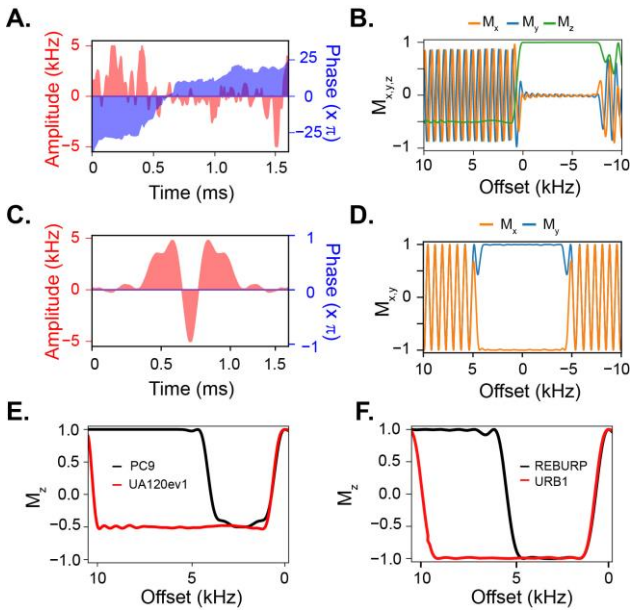

Fig. 1 AI-designed RF pulse shapes for excitation and refocusing operation. (a) Amplitude and phase profiles for UA120ev1. (b) Offset response of M_x, M_y, and M_z components of the magnetization after pulse execution for an initial state $\rho_{in} = M_z$. (c) Amplitude and phase profiles for URB1 pulse. (d) Offset response of the magnetization components to URB1. (e) Offset responses of the M_z component of magnetization for PC9 and UA120ev1 excitation pulses with a 120° tip angle. (f) Offset responses of the M_z component of the magnetization for REBURP and URB1. These pulses were simulated with no excitation/refocusing on-resonance and similar profiles near the water signal. To generate UA120ev1 and URB1, we set the flip angle at 120° and 180°, respectively. For both pulses, we input a bandwidth of 8 kHz, a maximum RF power of 5 kHz, RF compensation of ± 2%, and an average fidelity of 99%.

universal amide-selective 120° pulse with J evolution during its execution. Fig. 1A shows the UA120ev1 amplitude and phase versus time. In addition, Fig. 1B illustrates the simulated behaviors of the magnetization components (M_x, M_y, and M_z) as a function of the offset starting from an initial state M_z. The UA120ev1 pulse outperforms the PC9 pulse in terms of the bandwidth irradiated and uniformity of excitation as shown in Fig. 1C. Specifically, a UA120ev1 pulse of 1.6 ms covers a bandwidth of 9.2 kHz (Fig. 1C, red). In contrast, a PC9 pulse of 1.92 ms covers approximately 2.5 kHz (Fig. 1C, black). Also, the PC9 pulse has a lower uniformity profile across the excitation window, which causes the spin to be tipped at slightly different angles. Note that during the execution of the UA120ev1 pulse the chemical shifts and J coupling constants evolve for 90% of its length. In fact, the UA120ev1 pulse architecture is U(120) – 0.9 T_p, where U(120) is the RF operator for the 120° flipping operation, $e^{-i(2\pi/3I_x)}$, and T_p is the pulse duration. We then designed a second pulse to refocus the J_{HN} couplings during the t_1 evolution period. To accomplish this, we programmed GENETICS-AI to create a universal refocusing pulse (URB1 – Universal band-selective refocusing pulse) with a broader bandwidth than the original REBURP. Figs. 1D-1E show the calculated amplitude and phase profiles of the new URB1 pulse along with the simulated magnetization components (M_x and M_y) versus the offset. Fig. 1F shows a direct comparison between the two refocusing pulses as a function of the offset. The REBURP and URB1 pulses have an identical profile in the range of 0 to 3.6 kHz. However, URB1 covers a bandwidth of 8.1 kHz, which is more than double of that irradiated by the corresponding REBURP pulse. We then implemented both UA120ev1 and URB1 in the classical pulse sequence for the HMQC (Fig. 2) and tested its performance using a 350 μM sample of uniformly (U) ^{15}N labeled Raf Kinase Inhibitor protein (RKIP) (Fig. 3). To quantify the sensitivity gain, we compared the intensities of the U-^{15}N RKIP spectra acquired with SOFAST-HMQC and RAPID-HMQC pulse sequences under identical conditions (Fig. 3). Resonance intensities were evaluated by fitting each individual peak with a Gaussian (or Lorentzian) function using an in-house Python script. Notably, the RAPID-HMQC spectrum shows additional peaks that become detectable with AI-designed RF pulses. In particular, two resonances at approximately 11.1 and 12.2 ppm corresponding to the tryptophan indole resonances of RKIP are significantly more intense in the RAPID-HMQC compared to the SOFAST-HMQC spectrum (Figs. 3A-B). Similarly, resonances near the water signal (5.5-6.5 ppm) appear significantly more intense in the RAPID-HMQC spectrum. As expected, the resonances at the center of the amide region display similar intensities in both spectra. We then tested the performance of the SOFAST- and RAPID-HMQC as a function of the interscan delay (D_1). Fig. S1, ESI† shows the build-up of the average intensities for the two experiments along with the Fast-HMQC experiment using Ernst angle pulses.[19] The two LRE experiments display a significantly higher average intensities relative to the canonical HMQC experiment for short D_1, with the highest average intensity reached for D_1 = 0.3 sec. For D_1 values greater than 0.4 sec, both LRE experiments decrease in efficiency,[9] though they still perform significantly better than the Fast-HMQC sequence with Ernst angle pulses. A closer look at the buildup curves, however, shows that the RAPID-HMQC experiment is more sensitive, which is due to the broader bandwidth and the higher fidelity level. In the range of 0.1-0.5 sec, the gain in intensity ranges from 5-15% (Fig. S1 inset, ESI†). Fig. 4 shows a peak-by-peak

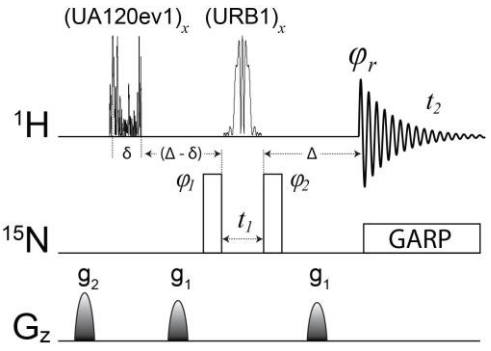

Fig. 2 RAPID-HMQC pulse sequence. The UA120ev1 pulse is the amide selective 120° pulse, with chemical shift and J evolution for 90% of the pulse length. Δ is set to 1/2J and δ = 0.9 × T_p. The URB1 pulse is the band-selective refocusing pulse. The phase cycles are as follows, ϕ_1 = x, -x; ϕ_2 = x, x, -x, -x; ϕ_r = x, -x, -x, x. The gradients are G1 = 7.3 and G2 = 23.1 Gauss/cm. The GARP sequence was used for broadband decoupling during the acquisition.

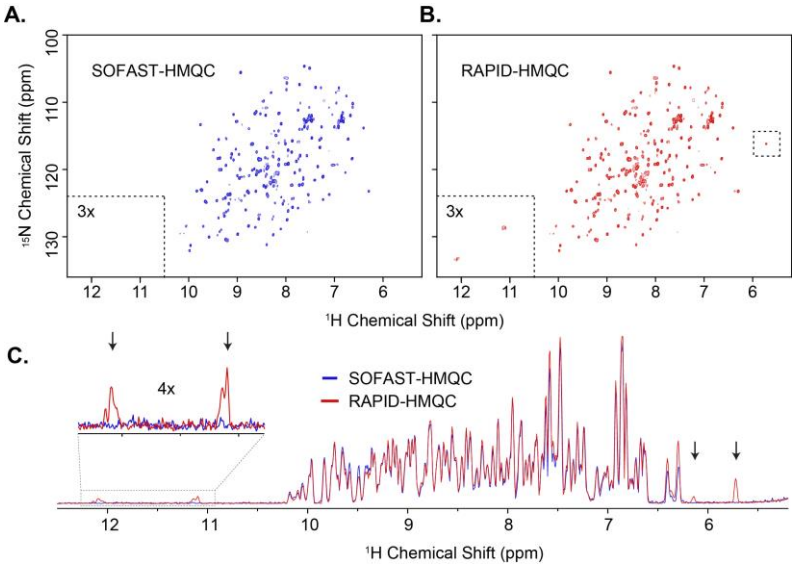

Fig. 3 Comparison of NMR spectra: (a) SOFAST-HMQC and b) RAPID-HMQC recorded using a 350 μM U-^{15}N labeled Raf Kinase Inhibitory Protein (RKIP) sample. The peaks highlighted in RAPID-HMQC are absent in SOFAST-HMQC. (c) Superposition of the 1D projections of the 2D spectra. The arrow indicates the resonances that are absent in SOFAST-HMQC. All spectra were recorded at 300 K on a Bruker 900 MHz spectrometer, using 8 scans and 16 dummy scans, with an interscan delay of 0.2 s. The complex FID data points have dimensions of 64 x 768 and were processed using NMRPipe, applying the sine bell apodization window with 0.4 offset. The data matrices were zero-filled to a final size of 512x2048.

comparison of the intensity ratios measured in the RAPID-HMQC and SOFAST-HMQC spectra, with PC9 and REBURP at increasing bandwidths. For a 2.1 kHz (3.5 ppm) bandwidth, the ^{1}H resonances of the SOFAST-HMQC spectrum at the edges of the low-field region are essentially undetectable, whereas the intensity of the peaks in the middle of the amide resonances is similar to the RAPID-HMQC spectrum. If the bandwidth of PC9 and REBURP is increased to 2.7 kHz (4.5 ppm), a few more peaks near the water signal are observed. However, the resonances at higher proton frequencies remain undetectable. The average values of the peak intensity ratio (I_{RAPID}/I_{SOFAST}) shows that there is a net gain of average intensity for the RAPID-HMQC experiments. When the bandwidth of the band-selective pulses is increased to 3.3 kHz (5.5 ppm), the SOFAST-HMQC spectra shows more peaks at the two edges. However, the I_{RAPID}/I_{SOFAST} ratios show a significant loss of sensitivity of the SOFAST relative to the RAPID-HMQC experiment. This loss of sensitivity is due to a partial irradiation of the water signal by the REBURP pulse, a shortcoming that was previously identified.[9] We repeated these experiments with an interscan delay of 0.5 sec and obtained similar results. We then plotted the average intensity normalized relative to the root-squared of the total experimental time ([number of scans + dummy scans] x [D_1 + duration of pulse sequence + acquisition time]) as a function of D_1 using the peak intensities of the canonical HMQC spectrum as a reference. We found that on average the RAPID-HMQC outperformed the SOFAST-HMQC experiment in a D_1 range of 0.01 to 0.6 sec. Finally, we tested the two LRE pulse sequences with one scan per t_1 point (no phase cycling), and for D_1 equal to 0.1 and 0.25 sec, for a total experimental time of 15 and 6 sec, respectively (Figs. S3 and S4, ESI†). In both experiments, we found that RAPID-HMQC has a higher signal-to-noise ratio for most of the resonances, and, for the 6 sec experiment, the suppression of the water signal is significantly better than the SOFAST-HMQC sequence (Fig. S4B, ESI†).

Overall, the new band-selective pulses designed for excitation and refocusing operations increase the sensitivity of the HMQC experiment, and unlike the SOFAST-HMQC, are better suited for high- and ultra-high magnetic fields. Note that the URB1 pulse can also be utilized for other pulse schemes. In fact, compared to the most commonly used refocusing pulses, *i.e.*, REBURP,[17] RSNOB,[20] Q3,[21] VEGA,[22] and the most recent SURBPOB180[23], the URB1 pulse covers a broader bandwidth and has a more uniform profile. To demonstrate this point, we simulated all pulses with identical duration (Fig. S5 ESI†). The REBURP, RSNOB, and Q3 pulses show narrow bandwidths for the refocusing operation with no modulation outside the region irradiated. The VEGA-180 pulse, on the other hand, irradiates a broader bandwidth (8.5 kHz), but it shows RF modulations outside the bandwidth irradiated, which restricts its applications beyond the LRE experiments. Finally, the SURBOP180[23] pulse developed using optimal control theory[24] covers a broader bandwidth (8.7 kHz), but, unlike the other refocusing pulses, the region outside its

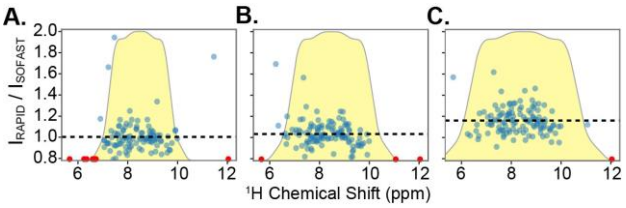

Fig. 4. Comparison of the U-^{15}N RKIP amide peak intensities of the RAPID-HMQC (I_{RAPID}) and SOFAST-HMQC (I_{SOFAST}) experiments with D_1 = 0.2 sec. The highlighted regions are the excitation bandwidths of SOFAST-HMQC. The SOFAST-HMQC experiments were acquired with band-selective pulses of (a) 3.5, (b) 4.5, and (c) 5.5 ppm bandwidths. Undetected peaks in the SOFAST-HMQC spectra are indicated as red dots. The dashed lines are the average values of I_{RAPID}/I_{SOFAST}.

irradiation bandwidth is narrower, which limits the ability to tune its bandwidth using lower power settings. Using the same settings, the URB1 refocusing pulse displays the largest bandwidth (11.4 kHz) and the highest level of fidelity. Its profile for the simulated magnetization component shows that outside the bandwidth irradiated there are no RF modulations, which makes this pulse generally applicable for spectroscopy as well as for imaging.

NMR spectroscopy at high and ultra-high magnetic fields calls for new RF pulses and pulse sequences.[25] In recent years, optimal control theory and optimization algorithms have played a critical role in pulse design.[24] GENETICS-AI is emerging as a new versatile approach for designing high-fidelity RF shapes for inversion, refocusing, excitation for broadband, and selective operations for solution[12, 26, 27] and solid-state[28] NMR spectroscopy. The excitation and the inversion pulses presented here are only examples of tailored RF pulse shapes that need to be implemented to improve the sensitivity and resolution of NMR applications at ultra-high magnetic fields.

Conclusions

We used a combination of an evolutionary algorithm and AI to design new band-selective pulses with high fidelity and broader bandwidth. When implemented in the [^{1}H,^{15}N] HMQC experiment, these new pulses enable the application of longitudinal ^{1}H relaxation-optimized experiments to high and ultra-high magnetic fields, where the breadth of the chemical shift is significantly large. We anticipate this new experiment will speed up the NMR application to characterize metabolites and biopolymers in living cells, taking advantage of the higher sensitivity and resolution at ultra-high magnetic fields. Additionally, it will contribute to the characterization of high-throughput screening as well as site-resolved, real-time analysis of kinetic processes.

This work was supported by the U.S. National Science Foundation (CHE-2304829) and by the Office of Discovery and Translation (ODAT) at the University of Minnesota. All experiments were conducted at the Minnesota NMR Center. The authors would like to thank Prof. M. Latham for critically reading the manuscript.

Author Contributions

Manu Veliparambil Subrahmanian calculated the RF shapes, simulated the RF effects on spin magnetization, implemented the pulse shapes and sequence into the NMR spectrometer, carried out data analysis, and wrote the first draft of the manuscript. Gianluigi Veglia conceived the project and experimental design, participated in the data analysis and interpretation, and wrote the paper.

Conflicts of interest

G.V. and M.V.S. are the founders of Kantika, LLC.

Notes and references

‡ Data, pulse sequences, and python code are available at https://conservancy.umn.edu/pages/drum/ and at https://github.com/manuvsub/RAPID-HMQC.

1. B. Brutscher and Z. Solyom, *New Dev Nmr*, 2017, **11**, 1-32.
2. M. Gal, P. Schanda, B. Brutscher and L. Frydman, *J Am Chem Soc*, 2007, **129**, 1372-1377.
3. P. Schanda, E. Kupce and B. Brutscher, *J Biomol NMR*, 2005, **33**, 199-211.
4. P. Schanda, H. Van Melckebeke and B. Brutscher, *J Am Chem Soc*, 2006, **128**, 9042-9043.
5. E. Luchinat, L. Barbieri, M. Cremonini and L. Banci, *J Biomol NMR*, 2021, **75**, 97-107.
6. S. Ghosh, A. Sengupta and K. Chandra, *Anal Bioanal Chem*, 2017, **409**, 6731-6738.
7. P. Schanda and B. Brutscher, *J Am Chem Soc*, 2005, **127**, 8014-8015.
8. R. Freeman, *Chem Rev*, 1991, **91**, 1397-1412.
9. P. Schanda, *Prog Nucl Mag Res Sp*, 2009, **55**, 238-265.
10. K. Pervushin, B. Vogeli and A. Eletsky, *J Am Chem Soc*, 2002, **124**, 12898-12902.
11. H. S. Atreya and T. Szyperski, *Proc Natl Acad Sci U S A*, 2004, **101**, 9642-9647.
12. V. S. Manu, C. Olivieri and G. Veglia, *Nat Commun*, 2023, **14**, 4144.
13. M. V. Subrahmanian, K. Pavuluri, C. Olivieri and G. Veglia, *PNAS Nexus*, 2022, **1**, pgac133.
14. W. P. Aue, E. Bartholdi and R. R. Ernst, *J Chem Phys*, 1976, **64**, 2229-2246.
15. A. J. Shaka, P. B. Barker and R. Freeman, *J Magn Reson*, 1985, **64**, 547-552.
16. E. Kupce and R. Freeman, *J Magn Reson Ser A*, 1994, **108**, 268-273.
17. H. Geen and R. Freeman, *J Magn Reson*, 1991, **93**, 93-141.
18. R. R. Ernst, G. Bodenhausen and A. Wokaun, *Principle of Nuclear Magnetic Resonance*, Claredon Press, Oxford, 1987.
19. A. Ross, M. Salzmann and H. Senn, *J Biomol NMR*, 1997, **10**, 389-396.
20. E. Kupce, J. Boyd and I. D. Campbell, *J Magn Reson B*, 1995, **106**, 300-303.
21. L. Emsley and G. Bodenhausen, *J Magn Reson*, 1992, **97**, 135-148.
22. D. Abramovich and S. Vega, *J Magn Reson*, 1993, **105**, 30-48.
23. S. Slad, W. Bermel, R. Kummerle, D. Mathieu and B. Luy, *Journal of Biomolecular Nmr*, 2022, **76**, 185-195.
24. N. Khaneja, T. Reiss, C. Kehlet, T. Schulte-Herbruggen and S. J. Glaser, *J Magn Reson*, 2005, **172**, 296-305.
25. J. H. Ardenkjaer-Larsen, G. S. Boebinger, A. Comment, S. Duckett, A. S. Edison, F. Engelke, C. Griesinger, R. G. Griffin, C. Hilty, H. Maeda, G. Parigi, T. Prisner, E. Ravera, J. van Bentum, S. Vega, A. Webb, C. Luchinat, H. Schwalbe and L. Frydman, *Angew Chem Int Ed Engl*, 2015, **54**, 9162-9185.
26. V. S. Manu, C. Olivieri, K. Pavuluri and G. Veglia, *Phys Chem Chem Phys*, 2022, **24**, 18477-18481.
27. V. S. Manu, C. Olivieri and G. Veglia, *J Biomol NMR*, 2023, **77**, 1-14.
28. T. Gopinath, V. S. Manu, D. K. Weber and G. Veglia, *Chemphyschem*, 2022, **23**, e202200127.